

# Nonlinear Regression-Based GNSS Multipath Dynamic Map Construction and Its Application in Deep Urban Areas

Yongjun Lee<sup>1b</sup>, Graduate Student Member, IEEE, Pai Wang<sup>2b</sup>, and Byungwoon Park<sup>1b</sup>, Member, IEEE

**Abstract**—GNSS signals are easily blocked or degraded because of the dense presence of high-rise buildings in urban areas, and positioning errors arising from reflected signals amount to as much as hundreds of meters. Various conventional GNSS techniques have been utilized to resolve this problem, but applying them to urban environments has been difficult owing to the complexity of the reflected signals and their unpredictable and nonlinear variation to the signal receiving environments. In this study, multipath maps were generated for dynamic users at multiple positions on a road and a residual-based map selection algorithm was implemented to solve the problem of user position uncertainty in deep urban environments. GNSS data collected over a period of 327 min were used to train the multipath maps corresponding to 247 points near the 2.5 km stretch of the Teheran-ro road in Seoul, South Korea. The proposed system performed efficiently—it was verified to be capable of constructing a multipath map with a radius of 25 m using only 4 min of data. Moreover, it improved positioning accuracy by 45 % horizontally and by 80 % vertically, enabling the determination of the positional information of an urban vehicle with a horizontal accuracy of 18 m during 99% of the duration of a one-hour-long dynamic test. Due to the nonreliance of the proposed method on prior information or implementation of additional sensors, it is expected to be widely used for constructing map-based multipath mitigation models as part of intelligent transportation infrastructure in all cities in future.

**Index Terms**—Deep urban area positioning, global navigation satellite system, multipath, non-line-of-sight error, support vector regression.

## I. INTRODUCTION

GLOBAL navigation satellite systems (GNSSs) are widely used in positioning, navigation, and timing services [1]

Manuscript received 31 December 2021; revised 11 June 2022, 17 October 2022, and 30 December 2022; accepted 2 February 2023. Date of publication 28 February 2023; date of current version 8 May 2023. This work was supported in part by the Ministry of Science and ICT (MSIT), South Korea, under the High-Potential Individuals Global Training Program, supervised by the Institute for Information and Communications Technology Planning and Evaluation (IITP), under Grant 2020-0-01531; and in part by the Unmanned Vehicles Core Technology Research and Development Program through the National Research Foundation of Korea (NRF) and the Unmanned Vehicle Advanced Research Center (UVARC) funded by MSIT under Grant 2020M3C1C1A01086407. The Associate Editor for this article was Z. Xiao. (Corresponding author: Byungwoon Park.)

Yongjun Lee and Byungwoon Park are with the Department of Aerospace Engineering and the Department of Convergence Engineering for Intelligent Drone, Sejong University, Seoul 05006, South Korea (e-mail: byungwoon@sejong.ac.kr).

Pai Wang is with the School of Electronic Information and Electrical Engineering, Shanghai Jiao Tong University, Shanghai 200240, China.

Digital Object Identifier 10.1109/TITS.2023.3246493

and are expected to be utilized as underlying technology in intelligent transportation systems (ITS) [2]. With the growing popularity of location-based services for citizens, e.g., smart devices, car navigation, and autonomous vehicles, the use of GNSS-based services has rapidly increased in densely populated urban areas. However, despite the concentration of GNSS-based services in urban areas, the signal reception environment in such regions is not favorable to GNSS, which makes its performance inaccurate, unreliable, and not robust. Satellite signals are consistently blocked, reflected, and diffracted by densely packed skyscrapers, which induce measurement errors known as multipath and non-line-of-sight (NLOS) errors. Multipath and NLOS errors are distinguished by whether a direct signal is received or not, and the error margins resulting from the two types of reception are quite different [3]. As reflected signal errors are site-specific errors that depend sensitively on surrounding environments and directions of satellite reception, they are very difficult to mitigate or model. In particular, the site-dependent nature of reflected GNSS signals makes them a dominant source of error in urban canyons—reflection against vehicles and buildings may cause positioning errors exceeding 100 m in some cases [4].

Unlike common GNSS errors, multipath and NLOS errors are site-dependent and cannot be eliminated using differential techniques, such as real-time kinematic (RTK) or differential GNSS (DGNSS). Various techniques have been used to achieve accurate and robust determination of positioning in urban canyons, which has been one of the most challenging issues in the field of GNSS for a long time. Classification and exclusion of reflected signals is a commonly implemented method. Increment of the number of GNSS signal sources are substantially improving the accuracy of conventional GNSS positioning even when reflected signals, especially NLOS ones, should be identified and excluded [5]. However, while reflected signals are usually of low strength, this may not always be the case in an urban area. In fact, signals reflected by windows of buildings, for instance, are occasionally stronger, making strong NLOS signals difficult to be distinguished from direct or LOS signals [6]. Techniques based on consistency checks of range measurement redundancy, e.g., receiver autonomous integrity monitoring (RAIM), cannot be implemented in urban environments easily to detect NLOS receptions either. This is because RAIM assumes that no more than one failure is detected at a time, which is not

true in urban environments—most signals received in an urban canyon are easily corrupted by multipath and NLOS errors [7]. Smoothing techniques based on carrier phase variation [8], [9] also enable more accurate positioning, but they require an accurate absolute position solution and a sufficient number of good signals for initialization [1], which are impractical and challenging requirements in urban environments [6].

The growing interest in machine learning and the potential of its application has also motivated several studies on its utilization in GNSS [10]. Machine learning-based techniques are tolerant of imprecise, partially incorrect, or uncertain data [11], and have the potential to detect relationships between data with high complexity, time variance, and nonlinearity that could not be modeled using explicit equations in physics or mathematics [12]. Compared to statistical methods, machine learning-based techniques enable us to identify dependencies in datasets whose underlying models have not been properly determined using exploratory analysis [10]. The most recently studied machine learning-based urban positioning technique was the multipath/NLOS signal classification technique. Machine learning-based techniques usually label the data based on the output of the receiver correlator or satellite measurement-based features and then classify the received signal following training. The signal correlator output [13], carrier-to-noise ratio (C/N0) obtained via right hand circular polarized (RHCP) and left hand circular polarized (LHCP) antennas [14], and satellite elevation angles have been used as input features during training, and various machine learning-based techniques such as neural network (NN), support vector machine (SVM) [13], decision tree (DT) [14], and k nearest neighbors [15] have been used to train the classification process. Recently, extraction of more accessible features from GNSS measurements has been attempted, and Doppler shift has emerged as a key feature in the classifier.

Various studies have been conducted to improve urban GNSS accuracy by combining machine learning-based classifiers with conventional GNSS positioning systems to mitigate the effect of reflected errors using probabilistic results obtained from classifiers. For instance, shadow matching performance was improved by excluding problematic satellites based on satellite visibility trained using SVM [16]. A multi-feature support SVM signal classifier was also suggested to improve the weighting scheme for GNSS measurements [17]. Owing to the advantage of better interpretation of the quality of GNSS observations based on features identified by the SVM classifier, the proposed weight scheme was observed to be superior to the traditional weight scheme in terms of modeling NLOS errors in GNSS measurements in urban environments. A convolutional neural network-based NLOS discriminator was also proposed to classify signals and modify the weighting method based on NLOS probability [18]. However, this method cannot ultimately eliminate reflected signal errors—it merely unweights them. So, it cannot serve as a solution for large multipath errors of hundreds of meters.

Machine learning-based techniques that estimate reflected signal errors directly improve accuracy by eliminating reflected signal errors without diminishing availability. Multipaths were directly connected by applying the iterative

properties of satellite orbits to machine learning in [19]. The conclusions of the study demonstrated that training a multipath estimation model using the multipath characteristics based on the repetitive satellite orbit of each satellite improves positioning accuracy compared to the general smoothing technique in an open-sky environment. The study modeled multipath signals based solely on the elevation and the azimuth of satellites in an open-sky environment instead of modeling urban multipaths based on complex and nonlinear characteristics. Another study proposed two variations of an algorithm for a gradient boosting decision tree (GBDT)-based pseudorange error prediction model based on elevation angle, C/N0, and pseudorange residuals to improve determination of position [20]. Its results demonstrated that although multipath/NLOS signal exclusion improves accuracy, it was sensitive to both the proximity and the geometrical configuration of the receiver and signal reflectors or blockers.

Multipath precomputation using 3D building information and ray-tracing technique was introduced to reduce the NLOS multipath impact [21]. While it was efficient enough to be run on a smartphone, LOS multipath could not be calculated and there is bound to be a difference between the theoretically simulated value and actual multipath error. In our previous work [22], a support vector regression (SVR)-based multipath model was proposed using real GNSS data and the relative geometry between users and satellites in deep urban areas. We generated a multipath map based on the azimuth and the elevation of each satellite using the directly extracted and estimated GNSS multipath error. An application of the error map to static users in deep urban areas exhibited a root mean square (RMS) error of less than 20 m. The proposed model was applicable to all multipath/NLOS/LOS signals without requiring classification of signal types and it directly eliminated ranging errors induced by the presence of reflection signals in pseudorange measurements. Since the distinction between multipath and NLOS error is meaningless for the suggested method, we collectively refer to both errors induced by these two reflected signals, i.e., LOS and NLOS signals, as multipaths.

Based on the previous results, this study proposes to generate multiple multipath maps for a dynamic user and to search an appropriate map despite user position uncertainty. In addition, the error model modification technique based on a building geometry is suggested to efficiently use the limited amount of data for realistically training the reflection error models. Training and test data were collected on roads in Seoul with the highest concentration of high-rise buildings to ensure the effectiveness of the model in environments with severe reflection signal reception. Finally, the position availability and accuracy of the error maps are also analyzed. The contributions of this paper are:

1. Construction of multipath maps at multiple points for dynamic users on straight roads and intersections in deep urban area
2. Efficiency improvement by the suggested map modification technique that enables small amount of GNSS data to train realistic multipath error models

3. Resolution of user position ambiguity when selecting a valid map among the generated multiple multipath maps

The remainder of this paper is organized as follows. In Section II, the multipath extraction methodology and model training are described. In Section III, the GNSS multipath map generation and adjustment algorithm for efficient dynamic map construction is introduced. Further, a dynamic map selection algorithm on the user side is presented and the field test results in urban canyons are examined. Finally, Section IV presents the discussion and conclusions.

## II. METHODOLOGY

### A. GNSS Observables and Multipath

GNSS code measurements represent the range obtained by multiplying the propagation time of the signal from the satellite to the receiver by the speed of light. The pseudorange code measurement of the  $i^{\text{th}}$  satellite at time  $t$  can be modeled using (1).

$$\rho^i(t) = d^i(t) + \left( B(t) - b^i(t) \right) + I^i(t) + T^i(t) + M^i + \epsilon_\rho^i \quad (1)$$

where  $d$  denotes the distance between the receiver and the satellite, and  $B$  and  $b$  denote the receiver and satellite clock errors, respectively.  $I$ ,  $T$ , and  $\epsilon_\rho$  denote the ionospheric error, tropospheric error, and noise, respectively. The superscript  $i$  indicates the pseudo-random noise (PRN) number of the satellite.

A reflected signal can distort the GNSS correlation peak generated by a direct signal, which can induce multipath interference amounting to half of a ranging code chip—approximately 150 m maximally [8]. On the other hand, when an NLOS signal is received in the absence of a direct signal, the receiver perceives it as the direct signal, inducing errors with no upper limit that can easily be as much as several kilometers. Thus, the ranges of the errors induced by LOS multipath interference and NLOS reflected signals are quite different; however, the two error terms are included in measurements in the same format and cause positioning errors in the same manner. In this paper, errors induced by both types of reflected signals, i.e., LOS and NLOS signals, are referred to as multipaths ( $M$ ).

GNSS common errors in the pseudorange, that is, atmospheric and satellite-related errors, can be mitigated via correction messages and pseudo-range correction (PRC,  $prc$ ). Reference station-free PRC is effective and convenient for vehicles with wide mobility, and corrections ( $prc_{SBAS}$ ) from a satellite-based augmentation system (SBAS) were used in this study, as included in (2). Because multipaths are site-dependent errors, the multipath error is still included in the corrected pseudorange ( $\tilde{\rho}$ ).

$$\tilde{\rho}^i(t) = \rho^i(t) + prc_{SBAS}^i \quad (2)$$

To provide accurate positional information to GNSS users in urban areas, multipath errors should be properly modelled and removed. Prior to multipath modelling, the multipath-induced errors in the GNSS observations should be extracted. The

multipath for each satellite can be calculated using (3), and calculation of the distance to the satellite ( $\hat{d}^i$ ) based on the rover's calculated position, estimated clock biases of the receiver ( $\hat{B}$ ), and the satellite ( $\hat{b}^i$ ) are necessary to extract the multipath. If the rover's position is not computed accurately, the accuracy of the distance and the clock bias are affected in the chain, resulting in inaccurate multipath error calculation using (3). Therefore, the extracted multipath in urban areas cannot be guaranteed to conform closely to reality.

$$M^i(t) \approx \tilde{\rho}^i(t) - \hat{d}^i(t) - \left( \hat{B}(t) - \hat{b}^i(t) \right) \quad (3)$$

### B. Multipath Extraction Methodology

Inaccurate determination of position in an urban area not only results in inaccurate distance calculation, but also ultimately induces inaccurate estimation of receiver clock error. When an external reference device is used, the distance  $\hat{d}^i$  can be computed with relatively small errors, whereas the clock bias  $\hat{B}(t)$  is not accurate owing to complications caused by the associated multipath error and cannot be independently computed based on the position of the external reference. Our previous study demonstrated that the clock bias estimated based on the least-square position,  $\hat{B}_{ls}(t)$ , is too biased and noisy to enable the extraction of unbiased multipath error from GNSS observables in environments with severe reflected signal reception [22].

Given that the multipath and clock bias estimation influence each other, this study estimated clock bias using high-elevation satellites with little risk of severe multipath error. The quasi-zenith satellite system (QZSS), a dedicated regional Japanese satellite system, is a good option for reliably estimating clock bias with little interference from multipaths. Because the signal from QZSS is transmitted from the near-zenith direction with an elevation angle more than  $70^\circ$  in the Asia-Pacific region [23], which can be reasonably assumed to be high enough for the signal to remain unaffected by multipaths, receiver clock bias can be calculated using (4).

$$\hat{B}^*(t) \approx \tilde{\rho}^*(t) - d^*(t) + b^*(t) \quad (4)$$

where the superscript,  $*$ , denotes a high-elevation QZSS satellite.

Now, replacing  $\hat{B}$  in (3) with  $\hat{B}^*$  obtained from (4) enables the extraction of unbiased multipaths free from  $\delta\hat{B}_{ls}$ , as described in (5).

$$M^i(t) \approx \tilde{\rho}^i(t) - d^i(t) - \left( \hat{B}^*(t) - b^i(t) \right) \quad (5)$$

QZSS was originally designed to complement the visibility and performance of GPS in urban canyons. To effectively improve satellite availability for the combined GPS+QZSS system [24], the QZSS clock is synchronized to GPS time, which enables QZSS clock bias estimates to be used for GPS multipath estimation without any adjustment. However, to estimate the multipath errors of other GNSS satellites than GPS or QZSS, it is necessary to compensate for the clock difference between GNSS and GPS/QZSS systems. After computing the time difference,  $TO_{GNSS|QZSS}$ , between the two systems with respect to a nearby reference station, as described in (6), the



multipath errors of other GNSSs can be obtained using (7).

$$TO_{GNSS|QZSS} = B_{GNSS} - B^* \quad (6)$$

$$M_{GNSS}^i(t) \approx \tilde{\rho}^i(t) - d^i(t) - \left( \hat{B}^*(t) + TO_{GNSS|QZSS} - b^i(t) \right) \quad (7)$$

### C. Multipath Estimation Model Training

GNSS signals transmitted from satellites along the same direction follow identical paths after being reflected against obstacle surfaces near the user's position. The multipath estimation model proposed in this paper predicts multipath assuming that the multipath distribution is determined by the relative position of the satellite with respect to the prediction point. The model is generally applicable to all satellites without requiring prior classification of multipath/NLOS/LOS signal types and is capable of predicting errors caused by reflected signals of all received satellites. Assuming that the user's exact position is known, the multipath error ( $M_{GNSS}^i$ ) is expressed as a function of the elevation ( $El^i$ ) and azimuth ( $Azi^i$ ) angles of the  $i$ -th satellite, as given by (8).

$$M_{GNSS}^i = f(El^i, Azi^i) \quad (8)$$

The training data were taken to be  $\{(\vec{x}_1, y_1), \dots, (\vec{x}_n, y_n)\} \in \mathbb{R}^2 \times \mathbb{R}$ , where the input data  $\vec{x}$  is a set of elevation and azimuth angles, and  $y$  denotes the multipath extracted using Eqs. (5) and (7). The multipath estimation model is given by (9):

$$f(\vec{x}) = \langle w, \vec{x} \rangle + b \quad (9)$$

where  $w \in R^2$  denotes the weighting vector, and  $b \in R$  denotes the bias vector.

The multipath estimation model was trained using SVR, which is a regression based on the SVM technique. SVM solves binary classification problems by formulating them as convex optimization problems, which entails estimating the maximum margin separating hyperplanes. The generalization of SVM to SVR is accomplished by introducing an  $\epsilon$ -insensitive region around the function, called the  $\epsilon$ -tube [25]. The optimization problem can be expressed by (10).

$$\begin{aligned} & \text{minimize} \frac{1}{2} \|w\|^2 + C \sum_{i=1}^N (\xi + \xi^*) \\ & \text{subject to} \begin{cases} y_i - \langle w, x_i \rangle - b \leq \epsilon + \xi \\ \langle w, x_i \rangle + b - y_i \leq \epsilon + \xi^* \\ \xi, \xi^* > 0 \end{cases} \end{aligned} \quad (10)$$

where the constant  $C > 0$  determines the tradeoff between flatness (a small  $w$ ) and the degrees to which the deviations larger than  $\xi$  are tolerated, and  $\xi$  and  $\xi^*$  are slack variables. After solving the optimization problem [26], the regression model can be expressed using (11):

$$f(x) = \sum_{i=1}^N w_i K(x, p_i) + b \quad (11)$$

where  $p_i$  denotes a support vector, and  $K$  denotes a kernel function. In this study, the Gaussian kernel given by (12) was selected because of its ability to handle nonlinearity [18].

$$(x_i, x_j) = \exp\left(-\frac{\|x_i - x_j\|^2}{2\sigma^2}\right) \quad (12)$$

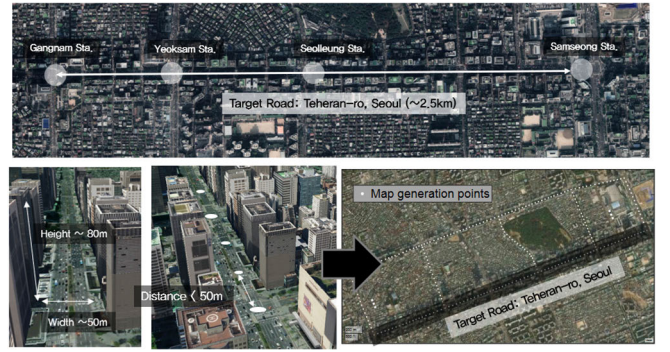


Fig. 1. Multipath dynamic map generation points on teheran-ro (Seoul, South Korea).

## III. RESULTS AND DISCUSSION

### A. Multipath Dynamic Map

Our previous study [22] suggested GNSS error mitigation technique using a multipath map which is defined as a polar contour-type map that indicates the estimated multipath for each elevation and azimuth angle  $360^\circ$  around one site. The estimated multipath on the map was trained using the relative position information of the user and the satellite. The model appropriately reflected the geometry of buildings near a static user in a deep urban area, and thus GNSS data collected over three hours—one hour each on three different days—were effective in improving the accuracy of static positioning in urban areas by 58.4 % horizontally and 77.7 % vertically, achieving an accuracy of 20 m in deep urban areas in Teheran-ro, Seoul [22]. The result showed the trained map was feasible to effectively mitigate each satellite error based only on the satellite elevation and azimuth angles in deep urban area regardless its constellation.

However, when the mobility of vehicles is considered, the multipath map at a static point becomes ineffective as an ITS technology. To improve the GNSS accuracy of a vehicle passing through the middle of an urban canyon, multipath maps should be continuously constructed at multiple points on the road, which is named as a multipath dynamic map. Collecting data from the as many points with as long durations as possible would enable the construction of a dynamic map almost continuously. However, the associated increase in big data can eventually lead to a significant increase in cost. Therefore, this study focuses on finding an efficient method that can be applied to resolve this problem practically in future traffic systems.

First, it is necessary to design the spacing between the map construction point effectively. Perception of a series of discrete maps as a continuous map is dependent on resolution, i.e., the distance over which the user can no longer distinguish the difference between successive maps even when the spacing between them is reduced further. Based on the 20 m RMS error of the user's horizontal position obtained in the previous static multipath study, user position accuracy can be expected to be slightly lower after the dynamic multipath map was applied—between 25 m and 30 m, approximately. Assuming that the horizontal positional error follows a Gaussian distribution, 95 % of the user's location would be distributed within approximately 50 m of the actual value. Therefore, even if the

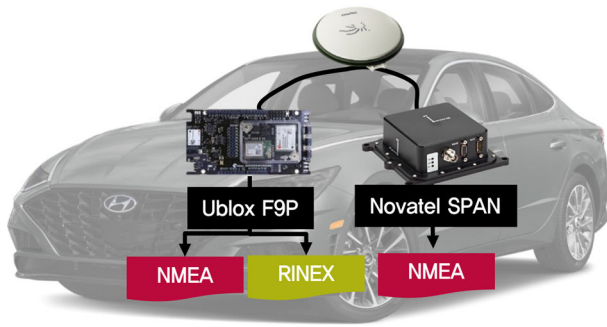


Fig. 2. GNSS data collecting vehicle.

spacing between successive maps were taken to be less than 50 m, the user is highly likely to be unable to apply the map that fits its position most closely. Thus, the spacing between the reference points for map construction was taken to be 50 m in this study.

The second requirement is the capability of constructing dynamic maps based on a small amount of data. Further, the data collecting vehicle must move continuously on the road where the speed limit is 14 m/s (50 km/h), only 3.6 s can be allocated to data collection for each map during a single run unless waiting for a signal or slowing down traffic.

### B. Multipath Dynamic Map Generation

We set multiple points to generate dynamic multipath maps on several roads and intersection in the Gangnam-gu, Seoul, near our target road, Teheran-ro. The target road was approximately 2.5 km long and 50 m wide from the Samseong to Gangnam subway stations and hosts several buildings that are 80 m or higher. The spacings between points corresponding to successive maps were set as 50 m to maintain a valid range for users using the dynamic multipath map. A total of 247 points were set on the roads in Gangnam-gu, and 53 points were located on the target road.

To collect the training data, a vehicle equipped with a GNSS receiver and a reference system was used, as depicted in Fig. 2. A U-blox ZED-F9P receiver was mounted on the vehicle to receive and store multi-constellation single-frequency pseudorange observables of GPS/GLONASS/BeiDou/GALILEO/QZSS in receiver independent exchange format. The mounted NovAtel SPAN-CPT equipment provided a continuous true reference trajectory of the vehicle in the National Marine Electronics Association (NMEA) format, even when GNSS signal reception was compromised.

Seven training datasets were collected at different times on different dates to construct the multipath estimation model at each map generation point, as detailed in Table I. GNSS data were logged over a period of 45 min approximately for each data set, and data collected over a total duration of 327 min were used for model training at 247 points.

Trajectories of seven training data and test data, and 247 map generation points are shown in Fig. 3. Training data were collected from trajectories passing through various roads in Gangnam-gu area to generate various maps with different road directions, and test data were collected around the target

TABLE I  
TRAINING DATASETS

Data Set	Data Collecting Period
Training Data 1	2021.03.30 05:00:00 ~ 05:45:00
Training Data 2	2021.07.20 08:30:00 ~ 09:15:00
Training Data 3	2021.07.28 03:00:00 ~ 03:45:00
Training Data 4	2021.08.04 07:45:00 ~ 08:30:00
Training Data 5	2022.04.11 07:45:00 ~ 08:30:00
Training Data 6	2022.04.11 15:45:00 ~ 16:30:00
Training Data 7	2022.04.18 16:00:00 ~ 16:45:00

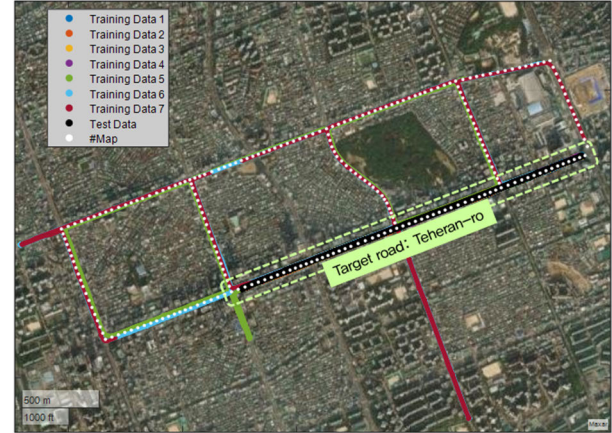


Fig. 3. Data collection trajectories and map generation point.

road. The logged training data was used to train multipath estimation model of the nearest generation point based on the reference trajectory.

The logged training data sets were used to train multipath estimation model and generate the multipath dynamic maps at the 247 points. The size of collected data was not uniform depending to the map generation point owing to partial traffic jams and signal waiting. After make-up drivings at relatively insufficient data collecting areas, the collected data sizes were mostly evenly distributed over the 53 points in target road, which is approximately 4.4 min data as illustrated in Fig. 4. Compared to our previous study [22], a single multipath map for dynamic users was trained using only 2.5% of the 171 min training data used for the previous static map construction.

As a consequence of the lower amount of data used for training, the total amount of the extracted multipath corresponding to each pair of elevation and azimuth angles was also much smaller compared to the previous study. Fig. 5 depicts the distributions of the estimated multipath data used for static and dynamic map learning at point #53. Even though more data for 15 min at the point #53 were used compared to the other points, the error distributions of the dynamic map looked very different from those of the static map. While the training data for the static map of the previous study were distributed as a conglomeration of continuous lines, the data for the dynamic map at point #53 were distributed as scattered dots, reflecting the discontinuous collection of training data.

Despite the absence of data continuity, the geometrical tendency of the estimated multipath could be ascertained from

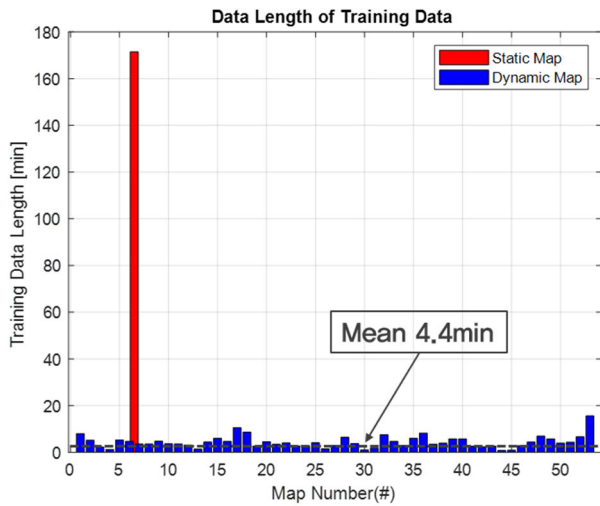


Fig. 4. Training data collected at each point on the target road.

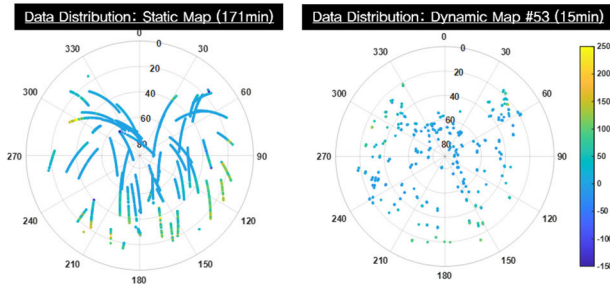


Fig. 5. Comparison of estimated multipath distributions for static (left) and dynamic (right) map construction.

the scattered dots. Similar to the tendency inferred from the continuous lines in the static multipath map, the multipath in the southeast and northwest directions, where buildings were located, was observed to be large. On the contrary, those in the direction above the road were very small, similar to that in the direction of the zenith. Despite being extracted from different satellites at different times, multipath values at the same point were similar, indicating the validity of the clock bias separation from the observation obtained using Eqs. (4)–(7). Thus, the multipath extracted via the proposed method is the unbiased multipath error. As the proposed method is not dependent on time or satellite constellation, data collected for multi-constellation at various times are preferable to the data for a single constellation collected continuously over a long period. It is the reason why the multi-constellation GNSS data for the map training were collected over 7 times separately, which enabled to efficiently construct the multipath dynamic map despite the short collection time of 4 min per single map.

Therefore, the following method can be used to construct an effective dynamic multipath map efficiently based on a small amount of data. First, the unbiased multipath should be extracted using the clock bias estimated using high elevation angle satellites. Moreover, measurements from various constellations collected over a long time interval or different time should be obtained to form training data observed from various satellite geometry.

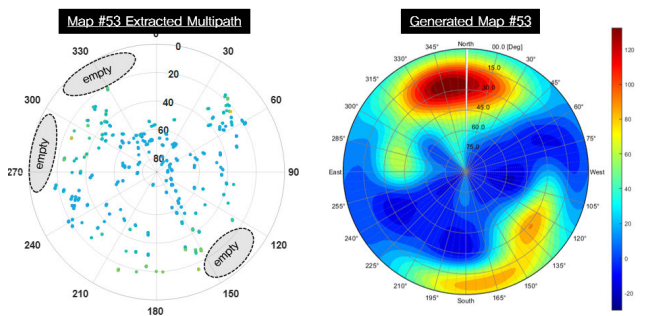


Fig. 6. Empty spaces in the extracted multipath samples (left) and the generated multipath Map (right).

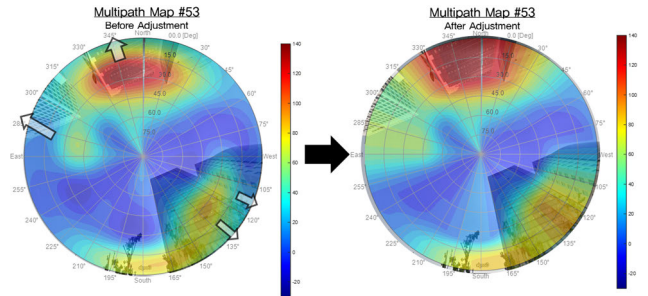


Fig. 7. Adjustment of multipath map.

C. Dynamic Multipath Map Adjustment

Despite the extraction of unbiased multipath errors via efficient data collection and time allocation, empty spaces were inevitably created due to the lack of training satellite data. The use of empty spaces as inputs to the SVR distorts the trained model. The left skyplot depicted in Fig. 6 illustrates the distribution of data used for learning the dynamic model at point #53, and the right diagram depicts the multipath map generated via nonlinear regression. According to the SVR model, the highest peak of the multipath errors corresponded to an azimuth of  $347^\circ$  and an elevation of  $25^\circ$ , and the surrounding multipath values decreased along the contour lines, even when the elevation angles decreased. Considering the geometrical arrangement of the actual buildings and their effects on the reflected signal, this result is unreasonable

In general, the elevation angle should be inversely proportional to the multipath [27], [28], [29]—thus, the severity of map distortion due to the lack of data is greater at low elevations than at high elevations. To rectify map distortion at low elevations, the empty spaces were filled in with the closest higher elevation data along the same azimuth. Fig. 7 depicts the modified multipath map obtained by adjusting the map generated using the model trained with an insufficient amount of data (left). The overlaps on the modified multipath map corroborate the validity of the adjustment. While, prior to adjustment, low multipaths were predicted at some points where satellite visibility was obviously blocked by buildings, this issue was resolved by the modification.

Figs. 8 and 9 depict examples of the modified multipath map at the points #1, #2, #11, and #12. As illustrated in Fig. 8, point #1 was located next to the intersection and exhibited relatively good visibility towards the east. The building geometry at this point could be easily inferred from the multipath map



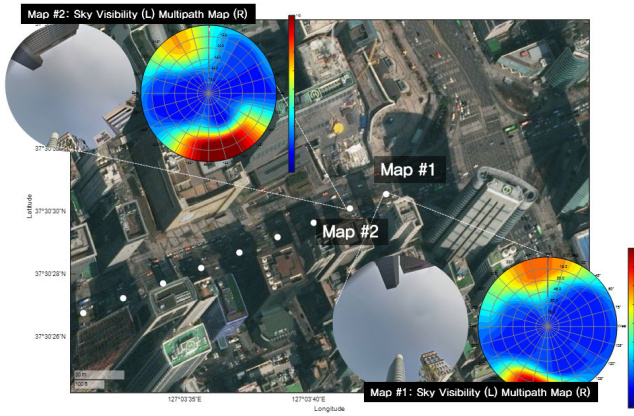


Fig. 8. Examples of modified multipath map (Map #1 and #2).

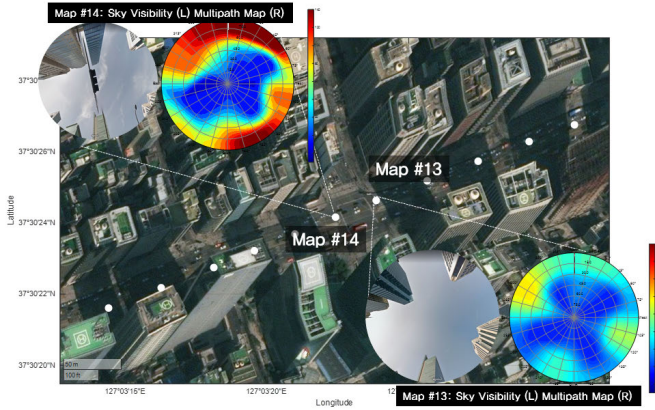


Fig. 9. Examples of modified multipath map (Map #13 and #14).

that predicted a lower multipath error towards the east. On the other hand, the map at point #2 revealed that the multipath error was expected to be large in both the north-west and south-east directions, which was supported by the overhead image of the building geometry.

As depicted in Fig. 9, Point #13 was located in the middle of an intersection with relatively good satellite visibility. The predicted multipaths were also mostly low, particularly over a cross-shaped zone contiguous with the road. Although point #14 was adjacent to point #13, the predicted multipath errors were high in the direction perpendicular to the road. This is because of the presence of very tall buildings—83–152 m in height—on that side that interfered with the signal.

#### D. Dynamic Map Selection Algorithm

Following the creation of the dynamic map by combining the multipath maps corresponding to 53 points on Teheran, a method is required to select the optimal map for each user. This is not an easy task because the uncertainty of the initial user position induces numerous candidates and iteration processes in existing multipath technologies [30], such as ray tracing or shadow matching. An appropriate iteration process is required in the case of the dynamic map as well to identify the optimal multipath map generated nearest to each vehicle's real position. If the exact position of the vehicle were known,

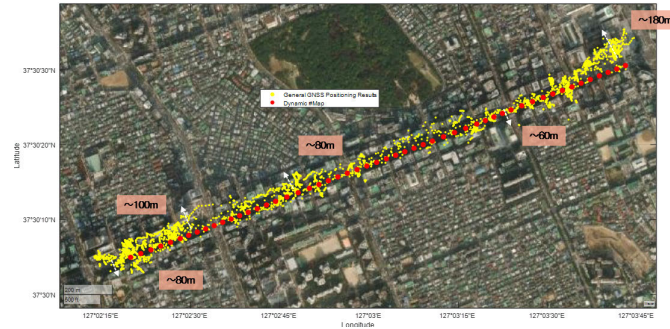


Fig. 10. Initially calculated user positions and multipath map generation points on target road.

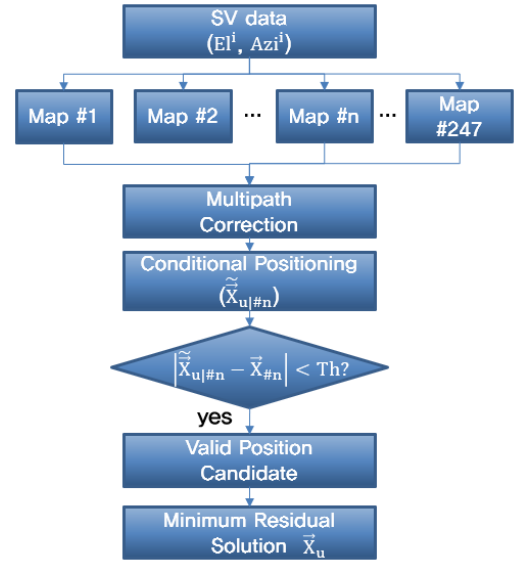


Fig. 11. Dynamic map selection algorithm on the user end.

then it would be possible to find the nearest optimal map based on the solved position, however there would be no need to apply a multipath map to the GNSS measurements observed at the vehicle. The problem lies in the fact that users in deep urban areas cannot calculate their positions accurately using GNSS solely, and thus cannot determine the maps that are optimal for them. As depicted in Fig. 10, vehicle positions were often found to exhibit larger errors than the spacing between successive multipath map generation points, i.e., 50 m, with the maximum error being 180 m. As NLOS multipath errors have no upper limit, it is impossible to predict how far maps from the initially computed position should be considered as candidates for the optimal map.

Thus, in severe multipath environments, all multipath maps should be considered as candidates for each user. An algorithm for selecting a map under uncertain conditions is presented in Fig. 11. As the real position of the user at time  $t$  is not known in severe NLOS environments in urban areas, all multipath maps are considered to predict the multipath of the  $i^{\text{th}}$  satellite at the user's position, and the predicted multipath error,  $M_{\#n}$ , is computed by inputting its elevation and azimuth angle,  $El$  and  $Azi$ , to model  $\#n$ . A conditional multipath-free pseudorange,  $\tilde{\rho}_{m.f|\#n}$ , can be acquired using (13). Using conditional multipath-free pseudoranges, the conditional

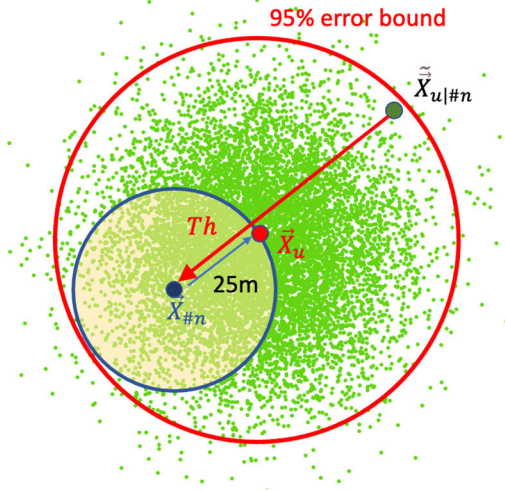


Fig. 12. Determination of valid range of multipath map.

multipath-mitigated position,  $\tilde{X}_{u|#n}$ , can be estimated.

$$\tilde{\rho}_{m.f|#n}^i(t) = \tilde{\rho}^i(t) - M_{\#n} \left( El^i(t), Az^i(t) \right) \quad (13)$$

If the selected map #n was generated near the user's location, the conditional position,  $\tilde{X}_{u|#n}$ , should be recursively placed near the point where the map #n was generated,  $\tilde{X}_{\#n}$ . Therefore, the conditional positions can be grouped as a valid position candidate if the distance between  $\tilde{X}_{u|#n}$  and  $\tilde{X}_{\#n}$  is within a valid range, as described by (14).

$$\left| \tilde{X}_{u|#n} - \tilde{X}_{\#n} \right| < Th \quad (14)$$

Because the distance between successive maps was taken to be 50 m, the effective radius of the map generated at  $\tilde{X}_{\#n}$  is 25 m. If the distance between the generation point,  $\tilde{X}_{\#n}$ , and the user's real position,  $\tilde{X}_u$ , is less than 25 m, the selected map #n can be considered to be appropriate for the user. Assuming that the calculated positive errors follow a Gaussian distribution, an additional range should be considered due to the error distribution to estimate the actual valid range,  $Th$ , as depicted in Fig. 12. As the user RMSE of the dynamic map was previously assumed to be 25 m and the 95 % error was 50 m, the valid range,  $Th$ , was taken to be 75 m.

The multipath mitigation is effective when its actual value at a user side is close to the modeled one. While NLOS multipath is not expected deviate much from the modeled one within the designed range, LOS multipath needs further investigation because it is caused by the interference between direct and non-direct signals. The amplitudes of the direct and reflected signals are combined, when they are in-phase to create a constructive multipath interference. This increases the signal intensity and creates a positive multipath error in the range-domain. Conversely, when the out-phase of the direct and reflected signals caused a destructive multipath interference, a negative ranging error occurs, and the measured signal strength decreased [31], [32]. Therefore, the user should detect if the current multipath error is caused by the destructive interference, because the modeled multipath map has been

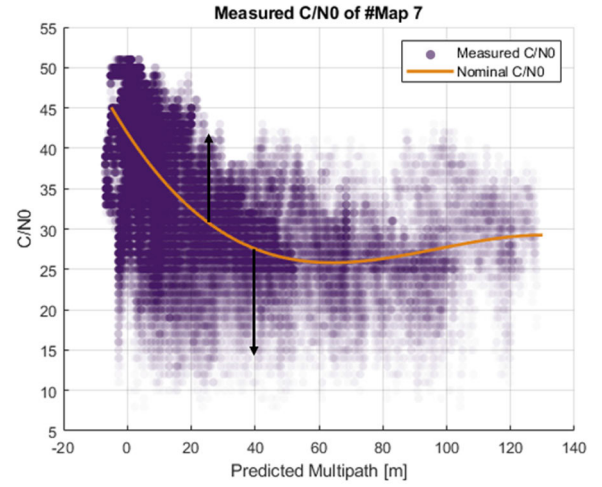


Fig. 13. Measured C/N0 and the calculated nominal C/N0 function for map #7.

constructed by the collected constructive multipath error data set.

C/N0, a signal strength-related term, is one of the indicators that can distinguish current multipath interference property. In an open-sky environment, C/N0 is usually proportional to the satellite elevation, but C/N0 with site-specific errors in an urban environment cannot be characterized by the elevation angle. In contrast, since the multipath is a site-specific error, the nominal C/N0 function can be created when the measured multipath errors are collected and processed at each point.

Figure 13 depicts a nominal C/N0 function modeled by the measured C/N0 for map #7. The measured C/N0 for each predicted multipath are marked with translucent purple dots. The area with higher dot density is colored darker, and as a result, the nominal C/N0 function of the orange line can be generated aligned with the belt that is the darkest. If the gap between the measured C/N0 at a rover side and the generated nominal C/N0 function value is found to be large, it can be regarded as a destructive multipath interference. Therefore, the difference between the measured and nominal C/N0, which is depicted as a black arrow in Figure 13, can be a metric to distinguish which interference, constructive or destructive, has induced the current multipath.

If a current multipath received at a user is due to constructive interference, the C/N0 of the received signal would be near to the nominal C/N0,  $C/N0_{nom|#n}$ , which is the generated model function,  $f_p$  in (15). Whereas the measured C/N0 will be much lower than the nominal value if a destructive multipath interference occurred at the user side.

$$C/N0_{nom|#n}(M_{\#n}) = f_p(M_{\#n}) \quad (15)$$

Figure 14 depicts the process of obtaining the nominal C/N0 function  $f_p$ . First, satellite elevation and azimuth are used to generate a multipath map #n, and a 3rd order polynomial function,  $f_p$ , is calculated using the multipath correction ( $M_{\#n}^i$ ) of the  $i$ -th satellite calculated from the multipath map #n and the C/N0 measurement of the  $i$ -th satellite ( $C/N0^i$ ).

To mitigate the influence of the unmodeled destructive multipath error, the corresponding satellite need to be de-weighted.



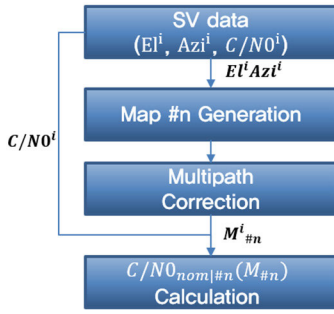


Fig. 14. Process of obtaining nominal C/N0 function.

The accuracy of site-specific unmodeled errors can be adaptively adjusted using the difference between received and modeled C/N0 values. In this work, a priori adaptive model suggested by Zhang et al. [33] was used to model the standard deviation of the multipath-mitigated pseudorange residual error,  $\sigma_{m.f.}$ . As shown in (16), valid measurements with effectively mitigated multipath errors would be primarily employed in positioning, whereas destructive interference measurements with large model errors would be de-weighted.

$$\begin{aligned} \sigma_{m.f.|\#n}^2 &= \sigma_{C/N0}^2 + \left| \sigma_{C/N0}^2 - \sigma_{C/N0_{nom}}^2 \right| \\ &= 10^{-\frac{C/N0}{10}} + \left| 10^{-\frac{C/N0}{10}} - 10^{-\frac{C/N0_{nom}(M_{\#n})}{10}} \right| \end{aligned} \quad (16)$$

Fig. 15 depicts an application of the multipath map selection algorithm on a user whose true position is located at a yellow dot on the google map. The user modelled the multipath errors for visible satellites using all the 247 maps and then get the conditional multipath-free pseudoranges ( $\tilde{\rho}_{m.f.|\#n}^i(t)$ ) to compute its conditional positions ( $\tilde{X}_{u|\#n}$ ), which are marked white dots in a white looped curve of Fig. 13 (a). Among the 247 conditional positions, only two conditional positions,  $\tilde{X}_{u|\#53}$  and  $\tilde{X}_{u|\#54}$ , were in the valid ranges of the multipath map #53 and #54, green and red dotted circle of Fig. 13 (b). In this way, the conditional position marked with green and red dots in Fig. 13 (b) were selected as valid position candidates.

The residual vector ( $\hat{v}$ ) for the conditional position can be expressed as (17).

$$\hat{v} = z - H\tilde{X}_{u|\#n} \quad (17)$$

where  $z$  and  $H$  represent the measurement vector including  $\tilde{\rho}_{m.f.|\#n}^i$  and navigation matrix, respectively. The residual square sums of the two valid candidates,  $\tilde{X}_{u|\#53}$  and  $\tilde{X}_{u|\#54}$  were 83.4 m and 75.2 m for 20 visible satellites, respectively. Finally,  $\tilde{X}_{u|\#54}$  which had the smallest residual sum was decided to be the final position,  $\tilde{X}_u$ . Its actual horizontal error was computed to be 1.4 m while the error of  $\tilde{X}_{u|\#53}$  was 17.5 m.

In contrast to the proposed method in this paper, shadow matching and ray tracing methods assign candidate maps near the initially calculated user positions based on 3-dimensional (3D) building information and then exclude or compensate for NLOS multipath errors. This requires an overwhelming amount of computation. While the iteration process based on

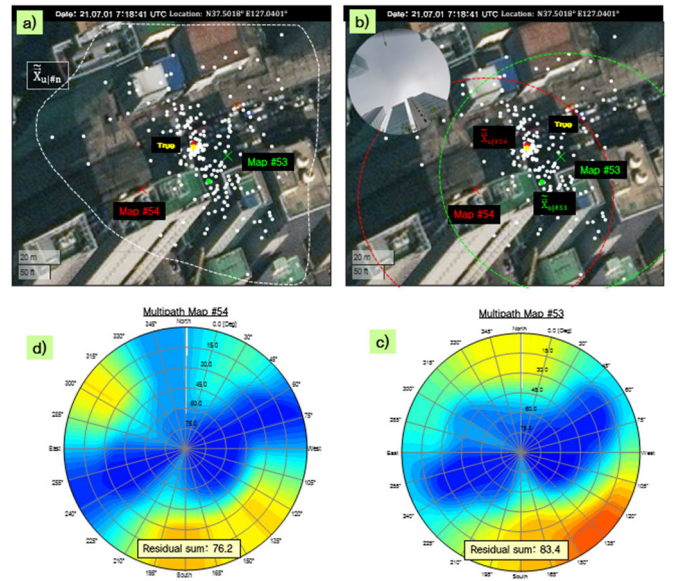


Fig. 15. Example of application of map selection algorithm ((a) Distribution of the computed conditional positions, (b) Valid ranges of multipath map #53 and #54, (c) Multipath map #53, (d) multipath map #54).

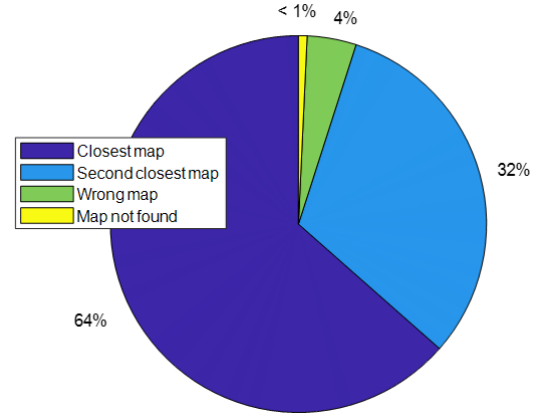


Fig. 16. Correctness of dynamically selected map.

3D building information should be performed independently, the iteration to apply multiple dynamic maps can be processed in parallel. The DGPS-CP [34], [35] method suggested in our previous works can conduct parallel iteration processing, which enables the projection of multiple multipath corrections from each map into the position domain and the direct correction of the initially calculated position. Therefore, the iteration process is not a hindrance to the application of dynamic multipath maps for urban users.

### E. Field Test Results

To verify the applicability of the algorithm in actual deep urban areas, a dynamic field test was performed in Tehran-ro, Seoul, Korea. The test data were collected over approximately one hour from 6:40 UTC on July 1, 2021. The configuration was identical to that during the collection of training data.

Corrections based on the selected multipath maps were applied and 99.3 % of the entire dataset were determined to be valid by (14). Among the positions determined to be valid, 64 % of the dynamically selected maps were the nearest maps from actual positions of the vehicle as depicted in Fig. 16.



Fig. 17. Horizontal positioning results for vehicle obtained using dynamic multipath map.

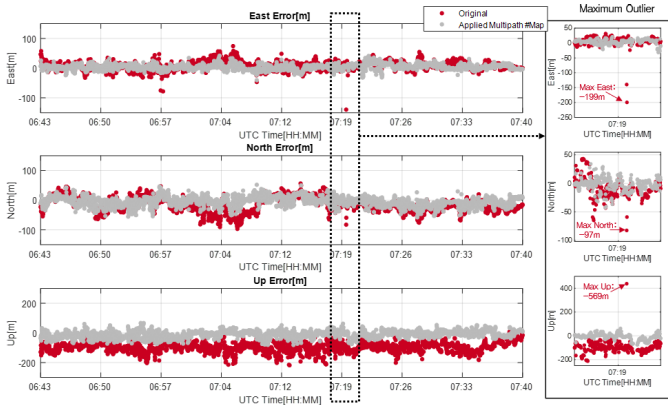


Fig. 18. ENU positioning obtained using dynamic multipath map.

Even though 32 % of the selected maps were not the closest ones but the second nearest ones, the user was mostly located between the selected and the nearest maps, and thus choosing either map would not have been wrong considering the error in user position. The averages of user horizontal errors for the nearest and second nearest map were 14.1 m and 17.5 m, respectively, which means the performance gap of the two cases was not seriously large.

The third nearest maps were selected during 4% of the test period, which was considered as a wrong map selected in this study. The average horizontal error for the wrong map case was only 16.2m, however its maximum error was up to 46.3m. Because of the large variance of the performance, the result is difficult to be expected as reliable as those of the previous two cases, but it is certain that the maximum error is to be limited less than  $Th$  of 75 m. During the remaining less than 1.0% of the test, the user failed to find its appropriate maps that passed the validity test of the conditional position in equation (14) despite searching all the generated maps.

Therefore, the results demonstrate that the residual-based map selection algorithm was mostly effective in identifying a valid map during the majority of the driving test.

Figs. 17 and 18 depict the vehicle's positions in horizontal and east-north-up (ENU) planes before and after mitigating the errors by applying the corrections from the selected dynamic

TABLE II  
ERRORS IN DYNAMIC MULTIPATH MAP POSITIONING

Positioning Method		MAX[m] (Improvement)	MEAN[m] (Improvement)	RMS [m] (Improvement)	95% [m] (Improvement)
Original	Horizontal	208.0	28.2	33.2	64.4
	Vertical	569.4	-92.3	92.8	148.4
Dynamic Multipath Map	Horizontal	65.9 (68.3%)	15.3 (45.7%)	18.4 (44.6%)	36.7 (43.0%)
	Vertical	81.1 (85.8%)	-9.3 (90.0%)	17.9 (80.7%)	48.6 (67.3%)

multipath maps. Before applying the dynamic multipath map, the horizontal and vertical RMSEs of the original positioning errors were 33.2m and 92.8 m, as summarized in Table II. The performance inconsistency at each position was very large owing to the site-dependent nature of multipaths; thus, it was difficult to estimate consistent error levels for urban positioning. The vertical errors were biased by -92.3 m, and the maximum errors in the horizontal and vertical planes were 208.0 m and 569.4 m, respectively.

On the other hand, the dynamic multipath map and residual-based selection algorithm improved the accuracy by 44.6 % horizontally and 80.7 % vertically, enabling a horizontal accuracy of 18.4 m and a vertical accuracy of 17.3 m. Further, the vertical bias was removed, resulting in an average error reduction of -9.3 m. The consistency of positioning performance was also significantly improved—it could be predicted within 45 m horizontally at most points, and the maximum error of approximately 600 m in three dimensions was reduced to less than 100 m. Considering that a 20 m horizontal RMSE was achieved for a static user using training data collected over 3 h, the method proposed in this study can be deemed to be very efficient, using only 2.5 % of the data used in the static case to improve the dynamic position accuracy in urban areas to similar levels.

#### IV. CONCLUSION

This paper proposed an effective algorithm for mitigating severe GNSS multipath errors for vehicles by constructing a set of dynamic multipath maps and selecting a valid map from it. The multipath map was generated based on multipath error prediction models at multiple points on Teheran-ro in Seoul, South Korea. As the error prediction model was trained using the relative geometry between the user and the satellites, it was capable of dealing with all kinds of reflected signal errors, i.e., LOS multipath and NLOS signal errors, without requiring prior classification. In addition, the model was trained by insufficient data and adjusted based on the geometrical arrangement of buildings and their effects on the reflected signal. Moreover, a user-end algorithm was proposed to reduce the risk of selecting an incorrect map corresponding to the user position owing to the uncertainty of the user's location. After applying all the generated maps to the vehicle's observables, maps that satisfied the recursion condition of the corrected position near the map generation point were selected. The final maps were verified to be those with the minimum residual error.

To validate the proposed algorithm and evaluate its performance in urban canyons, it was trained using total of 327 min of data to generate 247 multipath maps and conduct a dynamic test on a road named Teheran-ro in Seoul, South Korea with a length of 2.5 km and a width of 50 m. The results of the one-hour driving test revealed that the proposed algorithm improved positional accuracy by 45 % horizontally and 80 % vertically, yielding a horizontal RMS error of 18 m over 99 % of the duration of the session. The performance is similar to that in a static test, even though the model was trained using only approximately 2.5 % of the data used in static map construction.

The results obtained in this paper demonstrate that nonlinear and site-dependent urban multipath errors can be modeled without the help of additional information or sensors, such as 3D building information or cameras. The proposed multipath map construction technique is so efficient that it can be trained using only GNSS data collected over a mere 4 min over an area with 25 m radius. Therefore, it is expected to be widely used for constructing map-based multipath mitigating models in all cities. This model would contribute to the determination of the absolute position with an accuracy of 20 m immediately after turning on the GNSS receiver in the middle of an urban canyon. The instantaneous determination of absolute position is expected to be an important and solid foundation for integrating other sensors and information and for fitting data to provide accurate positions to various intelligent transportation systems in the future, such as smart mobility, drones, and even unmanned aerial mobility.

#### ACKNOWLEDGMENT

The authors would like to express their sincere gratitude to Prof. Y. Jade Morton and members of the Satellite Navigation and Sensing Laboratory at the University of Colorado Boulder for their insightful comments and suggestions on validation strategy for their machine learning algorithm.

#### REFERENCES

- [1] Y. Tian, M. Ge, and F. Neitzel, "Variance reduction of sequential Monte Carlo approach for GNSS phase bias estimation," *Mathematics*, vol. 8, no. 4, p. 522, Apr. 2020.
- [2] Y. Lee, Y. Hwang, J. Young Ahn, J. Seo, and B. Park, "Seamless accurate positioning in deep urban area based on mode switching between DGSS and multipath mitigation positioning," 2022, *arXiv:2206.04457*.
- [3] P. D. Groves, "How does non-line-of-sight reception differ from multipath interference," *Insid. GNSS*, vol. 8, pp. 40–42, Nov. 2013.
- [4] G. MacGougan et al., "Performance analysis of a stand-alone high-sensitivity receiver," *GPS Solutions*, vol. 6, no. 3, pp. 179–195, Dec. 2002.
- [5] M. Adjrad and P. D. Groves, "Enhancing least squares GNSS positioning with 3D mapping without accurate prior knowledge," *Navigation*, vol. 64, no. 1, pp. 75–91, Mar. 2017.
- [6] P. D. Groves, "It's time for 3D mapping aided GNSS," *Inside GNSS Magazine*, Sep. 1, 2016.
- [7] N. Zhu, J. Marais, D. Betaille, and M. Berbineau, "GNSS position integrity in urban environments: A review of literature," *IEEE Trans. Intell. Transp. Syst.*, vol. 19, no. 9, pp. 2762–2778, Sep. 2018.
- [8] J. Kim et al., "A low-cost, high-precision vehicle navigation system for deep urban multipath environment using TDCP measurements," *Sensors*, vol. 20, no. 11, p. 3254, Jun. 2020, doi: [10.3390/s20113254](https://doi.org/10.3390/s20113254).
- [9] B. Park and C. Kee, "The compact network RTK method: An effective solution to reduce GNSS temporal and spatial decorrelation error," *J. Navigat.*, vol. 63, no. 2, pp. 343–362, Apr. 2010, doi: [10.1017/S0373463309990440](https://doi.org/10.1017/S0373463309990440).
- [10] A. Siemuri, H. Kuusniemi, M. S. Elmusrati, P. Valisuo, and A. Shamsuzzoha, "Machine learning utilization in GNSS—Use cases, challenges and future applications," in *Proc. Int. Conf. Localization GNSS (ICL-GNSS)*, Jun. 2021, pp. 1–6.
- [11] R. Malhotra, "A systematic review of machine learning techniques for software fault prediction," *Appl. Soft Comput.*, vol. 27, pp. 504–518, Feb. 2015.
- [12] L.-T. Hsu, "What are the roles of artificial intelligence and machine learning in GNSS positioning?" *Inside GNSS*, Nov./Dec. 2020, pp. 20–27.
- [13] T. Suzuki and Y. Amano, "NLOS multipath classification of GNSS signal correlation output using machine learning," *Sensors*, vol. 21, no. 7, p. 2503, Apr. 2021.
- [14] B. Guermah, H. E. Ghazi, T. Sadiki, and H. Guermah, "A robust GNSS LOS/multipath signal classifier based on the fusion of information and machine learning for intelligent transportation systems," in *Proc. IEEE Int. Conf. Technol. Manage., Oper. Decisions (ICTMOD)*, Nov. 2018, pp. 94–100.
- [15] L.-T. Hsu, "GNSS multipath detection using a machine learning approach," in *Proc. IEEE 20th Int. Conf. Intell. Transp. Syst. (ITSC)*, Oct. 2017, pp. 1–6.
- [16] H. Xu, A. Angrisano, S. Gaglione, and L.-T. Hsu, "Machine learning based LOS/NLOS classifier and robust estimator for GNSS shadow matching," *Satell. Navigat.*, vol. 1, no. 1, pp. 1–12, Dec. 2020.
- [17] Z. Lyu and Y. Gao, "An SVM based weight scheme for improving kinematic GNSS positioning accuracy with low-cost GNSS receiver in urban environments," *Sensors*, vol. 20, no. 24, p. 7265, Dec. 2020.
- [18] T. Suzuki, K. Kusama, and Y. Amano, "NLOS multipath detection using convolutional neural network," in *Proc. 33rd Int. Tech. Meeting Satell. Division Inst. Navigat. (ION GNSS+)*, Oct. 2020, pp. 2989–3000.
- [19] Q. H. Phan and S. L. Tan, "Mitigation of GPS periodic multipath using nonlinear regression," in *Proc. 19th Eur. Signal Process. Conf.*, Aug. 2011, pp. 1795–1799.
- [20] R. Sun, G. Wang, Q. Cheng, L. Fu, and W. Y. Ochieng, "Improving GPS code phase positioning accuracy in urban environments using machine learning," *IEEE Internet Things J.*, vol. 8, no. 8, pp. 7065–7078, Apr. 2021.
- [21] X. Liu, S. Nath, and R. Govindan, "Gnome: A practical approach to NLOS mitigation for GPS positioning in smartphones," in *Proc. 16th Annu. Int. Conf. Mobile Syst., Appl., Services*, Jun. 2018, pp. 163–177, doi: [10.1145/3210240.3210343](https://doi.org/10.1145/3210240.3210343).
- [22] Y. Lee and B. Park, "Nonlinear regression-based GNSS multipath modelling in deep urban area," *Mathematics*, vol. 10, no. 3, p. 412, Jan. 2022, doi: [10.3390/math10030412](https://doi.org/10.3390/math10030412).
- [23] F. Wu, N. Kubo, and A. Yasuda, "A study on GPS augmentation using Japanese quasi-zenith satellite system," in *Proc. Position Location Navigat. Symp.*, 2004, pp. 347–356.
- [24] S. Zhu, D. Yue, L. He, Z. Liu, and J. Chen, "Comprehensive analysis of compatibility between QZSS and GPS in Asia-Pacific region: Signal quality, RTK and PPP," *Adv. Space Res.*, vol. 66, no. 2, pp. 395–411, Jul. 2020.
- [25] M. Awad and R. Khanna, "Support vector regression," in *Efficient Learning Machines*. Berkeley, CA, USA: Apress, 2015, pp. 67–80.
- [26] A. J. Smola and B. Schölkopf, "A tutorial on support vector regression," *Statist. Comput.*, vol. 14, no. 3, pp. 199–222, Aug. 2004.
- [27] K. Park and J. Seo, "Single-antenna-based GPS anti-jamming method exploiting polarization diversity," *IEEE Trans. Aerosp. Electron. Syst.*, vol. 57, no. 2, pp. 919–934, Apr. 2021.
- [28] M. Yoon and J. Lee, "Medium-scale traveling ionospheric disturbances in the Korean region on 10, November 2004: Potential impact on GPS-based navigation systems," *Space Weather*, vol. 12, no. 4, pp. 173–186, 2014.
- [29] B. Park, C. Lim, J. Wang, and Y. T. J. Morton, "Horizontal drift velocity and dimensions of ionospheric irregularities using ROT from a GNSS receiver array," *IEEE Trans. Geosci. Remote Sens.*, vol. 60, 2022, Art. no. 5803614, doi: [10.1109/TGRS.2022.3186839](https://doi.org/10.1109/TGRS.2022.3186839).
- [30] G. Zhang and L. Hsu, "Performance assessment of GNSS diffraction models in urban areas," *Navigation*, vol. 68, no. 2, pp. 369–389, Jun. 2021.
- [31] L. Lau and P. Cross, "A new signal-to-noise-ratio based stochastic model for GNSS high-precision carrier phase data processing algorithms in the presence of multipath errors," in *Proc. 19th Int. Tech. Meeting Satell. Division Inst. Navigat. (ION GNSS)*, 2006, pp. 276–285.



- [32] P. D. Groves, Z. Jiang, M. Rudi, and P. Strode, "A portfolio approach to NLOS and multipath mitigation in dense urban areas," in *Proc. 26th Int. Tech. Meeting Satell. Division Inst. Navigat.* Manassas, VA, USA: The Institute of Navigation, 2013, pp. 3231–3247.
- [33] Z. Zhang, B. Li, Y. Shen, Y. Gao, and M. Wang, "Site-specific unmodeled error mitigation for GNSS positioning in urban environments using a real-time adaptive weighting model," *Remote Sens.*, vol. 10, no. 7, p. 1157, 2018.
- [34] B. Park, J. Lee, Y. Kim, H. Yun, and C. Kee, "DGPS enhancement to GPS NMEA output data: DGPS by correction projection to position-domain," *J. Navigat.*, vol. 66, no. 2, pp. 249–264, Mar. 2013.
- [35] D. Yoon, C. Kee, J. Seo, and B. Park, "Position accuracy improvement by implementing the DGNSS-CP algorithm in smartphones," *Sensors*, vol. 16, no. 6, p. 910, Jun. 2016, doi: [10.3390/s16060910](https://doi.org/10.3390/s16060910).



**Yongjun Lee** (Graduate Student Member, IEEE) received the B.S. and M.S. degrees from Sejong University, South Korea, where he is currently pursuing the Ph.D. degree with the Department of Aerospace Engineering and the Department of Convergence Engineering for Intelligent Drone. His research interests include GNSS, multipath, urban positioning, and machine learning.



**Pai Wang** received the B.E. degree in information engineering and the Ph.D. degree in information and communication engineering from the Beijing Institute of Technology, Beijing, China, in 2012 and 2018, respectively. She was a Visiting Ph.D. Student with the School of Electrical Engineering and Telecommunications, University of New South Wales, Sydney, Australia, from 2015 to 2016. She was a Research Associate at the Smead Aerospace Engineering Sciences Department, University of Colorado Boulder, CO, USA, from 2018 to 2021. She is currently a tenure-track Associate Professor with the School of Electronic Information and Electrical Engineering, Shanghai Jiao Tong University, Shanghai, China. Her research interests include GNSS interference detection, mitigation, and localization, and navigation using signals-of-opportunity.



**Byungwoon Park** (Member, IEEE) received the B.S., M.S., and Ph.D. degrees from Seoul National University, Seoul, South Korea. From 2010 to 2012, he worked as a Senior and Principal Researcher at the Spatial Information Research Institute, Korea Cadastral Survey Corporation. Since 2012, he has been an Associate Professor with the School of Aerospace Engineering, Sejong University. He was a Visiting Professor at the Smead Aerospace Engineering Sciences Department, University of Colorado Boulder, CO, USA, from 2018 to 2020. His research interests include wide area DGNSS (WAD) correction generation algorithms, geodesy, real-time kinematics (RTK)/network RTK related algorithms, and estimation of ionospheric irregularity drift velocity using ROT variation and spaced GNSS receivers.